IJCPE
Iraqi Journal of Chemical and Petroleum Engineering

Iraqi Journal of Chemical and Petroleum Engineering
Vol.12 No.4 (December 2011) 5-20
ISSN: 1997-4884

University of Baghdad
College of Engineering

Laminar Free Convection in Three Dimensional Inclined Porous Annulus with Fins on the Inner Cylinder

Saad M. AL-Mashaat and Manal H. AL-Hafidh
University of Baghdad

Abstract

An experimental and numerical study was carried out to investigate the heat transfer by natural convection in a three dimensional annulus enclosure filled with porous media (silica sand) between two inclined concentric cylinders with (and without) annular fins attached to the inner cylinder under steady state condition. The experiments were carried out for a range of modified Rayleigh number ($0.2 \leq Ra^{*} \leq 11$) and extended to $Ra^{*}=500$ for numerical study and for annulus inclination angle of ($\delta = 0^{\circ}, 30^{\circ}, 60^{\circ}$ and 90°). The numerical study was to give the governing equation under assumptions that used Darcy law and Boussinesq's approximation and then it was solved numerically using finite difference approximation. It was found that the average Nusselt number depends on (Ra^{*}, Hf, δ and Rr). The results showed that the increasing of the fin length increases the heat transfer rate for any fin pitch unless the area of the inner cylinder exceeds that of the outer one; then the heat will be stored in the porous media. A comparison was made between the results of the present work and those of other researches for the case without fins and excellent agreement was obtained.

الخلاصة:

أجريت في هذا البحث دراسة عملية ونظرية لإنتقال الطاقة الحرارية بالحمل الحر في فجوة حلقية ثلاثية الأبعاد مملؤة بوسط مسامي(رمل) بين أسطوانتين مائلتين متحدتي المركز بوجود (وعدم وجود) زعانف متصلة بالإسطوانة الداخلية تحت شروط حالة الإستقرار. أجريت التجارب العملية لمدى عدد رالي المعدّل ($0.2 \leq Ra^{*} \leq 11$) ولمدى $Ra^{*}= 500$ في الجزء النظري ولزاوية ميل ($\delta = 0^{\circ}, 30^{\circ}, 60^{\circ}$ and 90°). تم كتابة المعادلات الحاكمة في الدراسة النظرية تحت فرضيات قانون دارسي وتقريب بوسنسك وتحويلها الى معادلة بدلالة الجهد المتجه والتي بدورها حلت عدديا باستخدام طريقة الفروق المحددة. تتضمن إمكانية الحل العددي حساب الجهد المتجه ودرجة الحرارة وعدد نسلت الموقعي والمتوسط. بينت النتائج أن عدد نسلت المتوسط يعتمد على عدد رالي المعدّل وطول الزعنفة وزاوية ميل الأسطوانة ونسبة الأقطار, بينت النتائج أن زيادة طول الزعنفة لأي خطوة زعنفة يسبب زيادة في أنتقال الطاقة الحرارية إلا في حالة زيادة المساحة السطحية للأسطوانة الداخلية على تلك التي للأسطوانة الخارجية فإن ذلك يتسبب في خزن الطاقة الحرارية في الوسط المسامي. قورنت النتائج للبحث الحالي مع نتائج بحوث أخرى في حالة عدم وجود زعانف وأعطت توافق جيد.

Key Words: natural convection, three dimensional, inclined annulus, porous media and annular fins.

Introduction

In recent years, natural convection in a cylindrical annulus has attracted much attention in relation to solar collectors, thermal storage systems and spent nuclear fuel cooling. A review of the works concerning this configuration was presented by Kuehn and Goldstein [l]. However, most of them were for horizontal concentric cylinders with infinite axial length. In this case, a two-dimensional (2-D) analysis is allowed because the convective flow is confined to the vertical plane and the flow pattern is identical in each annular cross section. On the other hand, a three dimensional (3-D) treatment is unavoidable in the horizontal case with the finite axial length and the rigid axial boundary surfaces and/or in the case when the cylinders are inclined from the horizon, because the viscous shearing force at the end walls and/or the gravitational force have an effect on the convection toward the axial direction **Fukuda [1]**.

In the 3-D numerical analysis, the matrix to be dealt with is far larger than that in the 2-D case, taking more CPU time to obtain the solution. Recently it has become feasible to treat this problem due to improvements in processing speed and memory capacity of digital computers. Several numerical works have been performed, most of them for rectangular enclosures. Numerical analysis has been performed by **Fukuda [1]** on three dimensional natural convection enclosed with concentric inclined cylinders. Governing equations were numerically solved by means of over – relaxation method for ranges of RaDa (a product of Rayleigh number Ra and Darcy number Da) from 1 to 1000 and an angle of inclination of cylinders from the horizon of 0 to $\pi/2$. Results showed that the local Nusselt number on the inner cylinder wall has its maximum value at bottom end, while Nusselt number on the outer cylinder wall has its maximum value at top end. However, the average Nusselt number depends largely on only RaDa and is hardly affected by the inclination.

Bogdan [2] presented experimental and numerical work investigating the effect of metallic porous materials, inserted in a pipe, on the rate of heat transfer. The pipe is subjected to a constant and uniform heat flux. The effects of porosity, porous material diameter and thermal conductivity as well as Reynolds number on the heat transfer rate and pressure drop are investigated. The results are compared with the clear flow case where no porous material was used. It is shown that for an accurate simulation of heat transfer when a porous insert is employed its effective thermal conductivity should be carefully evaluated.

Ramón [3] numerically investigated three-dimensional natural convection of air in a cubical enclosure with a fin on the hot wall for Rayleigh numbers of 10^3–10^6. The fin, with a thickness of 1/10 of the cavity side, is placed horizontally on the hot wall. The solid to fluid thermal conductivity ratio (R_k) and the fin width are varied. Because the fin is shorter than the cavity side, the cold flow sweeps the lower fin face and the hot wall at the clearances between the fin sides and the lateral walls, where high vertical velocities are reached. The fin inhibits the frontal and lateral access of fluid to the upper fin face, especially at low Rayleigh numbers. Low values of R_k cause heat transfer reductions. The contribution of the fin faces increases at high R_k causing heat transfer enhancements above 20%, which exceed the ones obtained in most two-dimensional studies. In the range of Ra from 10^5 to 10^6, maximum heat transfer rates are found for dimensionless fin widths of 0.6 and 0.8 respectively. It is

concluded that for $10^5 \leq Ra \leq 10^6$ a fin of partial width is more effective in promoting heat transfer than a fin of full width.

Experimental Study

Three outer cylinders of different diameters were manufactured to vary the radius ratio and to vary the fin length; ten inner cylinders were manufactured one without fins and the others with different fin length(Hf =3mm, 7mm and 11mm), radius ratios of ($Rr=(r_1/r_2)$ = 0.293, 0.364 and 0.435), number of fins (n=12, 23 and 45) and pitch length of (s = 19.2mm, 8.4mm and 3mm) to investigate the effect of these parameters and the effect of modified Rayleigh number by the variation of the temperature difference between the two concentric cylinders by means of a variable electric input power. Aluminum was chosen because of its high thermal conductivity and easy machinability. The test section consists of a three Aluminum outer cylinders of (100 mm), (82 mm) and (70 mm) outside diameters, (4 mm) thick and (260mm) long to which ten Aluminum inner cylinders of (27mm) outside diameter, (260 mm) long and (5 mm) thick. The inner cylinder was heated by passing an alternating current to a heater inside the inner cylinder and the outer cylinder was subjected to the surrounding temperature (freezer) where the minimum temperature was 270 K. The inner cylinder surface temperatures were measured at six locations using thermocouples type (K). The experimental apparatus is shown diagrammatically in **Fig. 1**

Mathematical Model

The schematic drawing of the geometry and the Cartesian coordinate system employed in solving the problem is shown in **Fig. 2.**

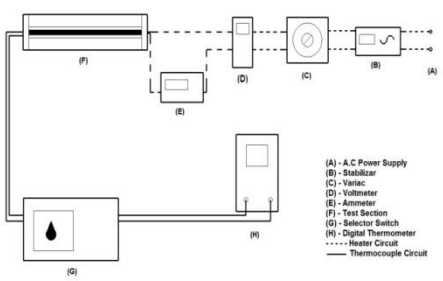

Fig.1, Schematic Diagram of Experimental Apparatus

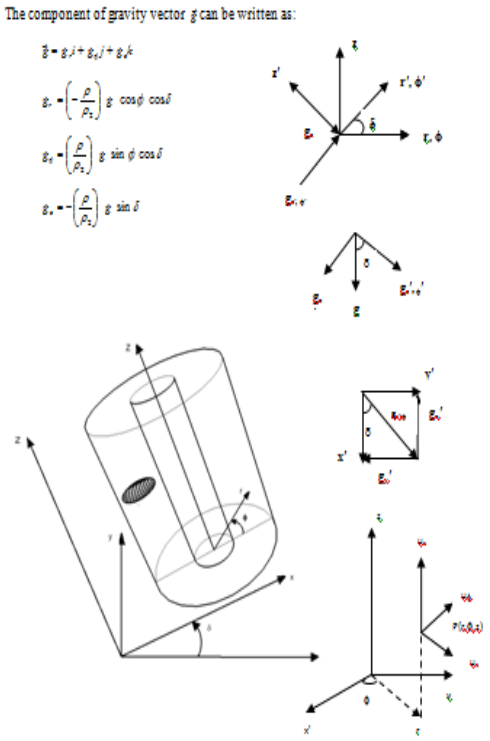

(a)

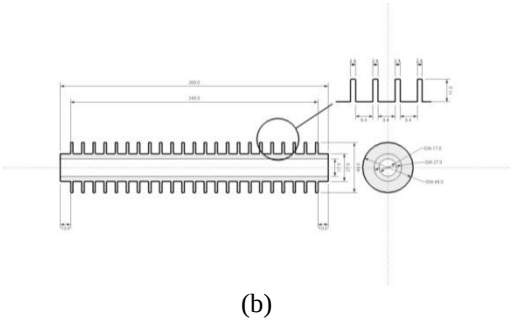

(b)

Fig. 2, (a) Geometry and coordinates system and (b) Schematic Diagram of Inner Cylinder with 8.4mm pitch

In order to model the incompressible flow in the porous medium, the steady-state equations of the Darcy flow

model, namely, the mass, the momentum (Darcy), the energy conservation laws and the Boussinesq's approximation are employed. These equations in vectorial notation are given by **Nield and Bejan [4]** and fin equation by **Ramón [3].**

Governing Equations

The conservation equations of mass, momentum and energy in steady state and the supplementary equation are **Fukuda [1]**:

$$\rho = \rho_2 \{1 - \beta(T - T_2)\} \quad (1)$$

Where:

$$\beta = \frac{1}{\rho}\frac{\partial \rho}{\partial T} \quad (2)$$

β is the thermal coefficient of the volume expansion; this constant is evaluated at T_2 which is the temperature at the inner surface of the outer cylinder, ρ_2 is the density at T_2 and ρ is the density at T, **Fukuda [1]**. This technique is called Boussinesq's approximation.

Mass Conservation

$$\frac{\partial u_r}{\partial r} + \frac{u_r}{r} + \frac{1}{r}\frac{\partial u_\phi}{\partial \phi} + \frac{\partial u_z}{\partial z} = 0 \quad (3)$$

Momentum Equations

The most common model used for flow in the porous media is the Darcy flow model. Darcy's law states that the volume average velocity through the porous material is proportional with the pressure gradient. In three dimensional flows, the Darcy's model **Wang [5]** is:

Momentum Equation in Radial Direction

$$u_r = \frac{K}{\mu_f}\left[-\frac{\partial p}{\partial r} - \rho\, g\, \cos\phi\, \cos\delta\right] \quad (4)$$

Momentum Equation in Angular Direction

$$u_\phi = \frac{K}{\mu_f}\left[-\frac{1}{r}\frac{\partial p}{\partial \phi} + \rho\, g\, \sin\phi\, \cos\delta\right] \quad (5)$$

Momentum Equation in Axial Direction

$$u_z = \frac{K}{\mu_f}\left[-\frac{\partial p}{\partial z} - \rho\, g\, \sin\delta\right] \quad (6)$$

Energy Equation

$$\frac{\partial(\rho\, C_p T)}{\partial t} + u_r \frac{\partial}{\partial r}(\rho\, C_p T) + \frac{u_\phi}{r}\frac{\partial}{\partial \phi}(\rho\, C_p T) + u_z \frac{\partial}{\partial z}(\rho\, C_p T) = \frac{1}{r}\frac{\partial}{\partial r}\left\{r\frac{\partial(k\, T)}{\partial r}\right\} + \frac{1}{r^2}\frac{\partial^2(k\, T)}{\partial \phi^2} + \frac{\partial^2(k\, T)}{\partial z^2} + \mu\, \Phi \quad (7)$$

Where Φ is viscous dissipation function.

Fin Equation

Within the fin itself, the energy equation is **Ramón [3]:**

$$\frac{\partial T}{\partial r} + \frac{T}{r} + \frac{1}{r}\frac{\partial T}{\partial \phi} + \frac{\partial T}{\partial z} = 0 \quad (8)$$

Following **Aziz [6]** a vector potential Ψ with its components:

$$\Psi = (\psi_r,\ \psi_\phi,\ \psi_z))$$

Defined by:

$$U = \alpha_{eff.}\ \nabla\ \mathrm{X}\ \Psi \quad (9)$$

$$\nabla^2 \psi_r = \frac{1}{R}\frac{\partial U_z}{\partial \phi} - \frac{\partial U_\phi}{\partial Z} \quad (10)$$

$$\nabla^2 \psi_\phi = \frac{\partial U_r}{\partial Z} - \frac{\partial U_z}{\partial R} \quad (11)$$

$$\nabla^2 \psi_Z = \frac{1}{R}\frac{\partial(R U_\phi)}{\partial R} - \frac{1}{R}\frac{\partial U_r}{\partial \phi} \quad (12)$$

Non Dimensional Variables

The characteristic length for the present study is r_2 **Fukuda [1]** to convert the governing equations to the dimensionless form, the dimensionless magnitudes must be defined as follow:

$$R=\frac{r}{r_2},\qquad Z=\frac{z}{r_2},\qquad U_r=\frac{u_r\ l}{\alpha_m},$$

$$U_\phi=\frac{u_\phi\ l}{\alpha_{eff}},\qquad U_z=\frac{u_z\ l}{\alpha_{eff.}},$$

$$\theta=(T-T_2)/(T_1-T_2),\quad P=\frac{p\ K\ l}{\alpha_{eff}\ \mu_f\ r_2}$$

$$Ra^*=g\ \beta\ K\ (T_1-T_2)\ (r_2-r_1)/\alpha_{eff.}\ \upsilon$$

$$,\ S_1=\frac{s}{2\ r_2},\ S_2=\frac{\frac{s}{2}+t}{r_2}\quad H_1=\frac{H_f}{r_2}$$

Substitute these dimensionless magnitudes in the governing equations.

Alternative expressions of Eq. (3) may be written in terms of $\psi_r,\ \psi_\phi$ *and* ψ_z *as*:

$$U_r=\left(\frac{1}{R}\frac{\partial\psi_z}{\partial\phi}-\frac{\partial\psi_\phi}{\partial Z}\right) \tag{13}$$

$$U_\phi=\left(\frac{\partial\psi_r}{\partial Z}-\frac{\partial\psi_z}{\partial R}\right) \tag{14}$$

$$U_z=\frac{1}{R}\left\{\frac{\partial}{\partial R}(R\ \psi_\phi)-\frac{\partial\psi_r}{\partial\phi}\right\} \tag{15}$$

Taking curl of momentum equations to eliminate pressure terms, the momentum equations will be:

$$Ra^*\ \frac{l}{(r_2-r_1)}\left(\frac{1}{R}\sin\delta\frac{\partial\theta}{\partial\phi}+\sin\phi\ \cos\delta\frac{\partial\theta}{\partial Z}\right)=$$

$$-\frac{\partial^2\psi_r}{\partial R^2}-\frac{1}{R^2}\frac{\partial(R\psi_r)}{\partial R}-\frac{2}{R}\frac{\partial\psi_r}{\partial R}-\frac{1}{R^2}\frac{\partial^2\psi_r}{\partial\phi^2}$$

$$-\frac{\partial^2\psi_r}{\partial Z^2}-\frac{2}{R}\frac{\partial\psi_z}{\partial Z} \tag{16}$$

$$Ra^*\ \frac{l}{(r_2-r_1)}\left(\cos\phi\ \cos\delta\frac{\partial\theta}{\partial Z}-\sin\delta\frac{\partial\theta}{\partial R}\right)=$$

$$-\frac{\partial^2\psi_\phi}{\partial Z^2}-\frac{\partial^2\psi_\phi}{\partial R^2}-\frac{1}{R^2}\frac{\partial^2\psi_\phi}{\partial\phi^2}$$

$$-\frac{2}{R^2}\frac{\partial\psi_r}{\partial\phi}+\frac{\psi_\phi}{R^2}-\frac{1}{R}\frac{\partial\psi_\phi}{\partial R} \tag{17}$$

$$-Ra^*\ \frac{l}{(r_2-r_1)}\cos\delta\left(\frac{1}{R}\cos\phi\frac{\partial\theta}{\partial\phi}+\sin\phi\frac{\partial\theta}{\partial R}\right)=$$

$$-\frac{\partial^2\psi_z}{\partial R^2}-\frac{1}{R}\frac{\partial\psi_z}{\partial R}-\frac{1}{R^2}\frac{\partial^2\psi_z}{\partial\phi^2}-\frac{\partial^2\psi_z}{\partial Z^2} \tag{18}$$

The vector potential equation was obtained in the dimensionless form as

$$\nabla^2\psi_r=-\frac{\partial^2\psi_r}{\partial R^2}-\frac{1}{R^2}\frac{\partial(R\ \psi_r)}{\partial R}$$

$$-\frac{2}{R}\frac{\partial\psi_r}{\partial R}-\frac{1}{R^2}\frac{\partial^2\psi_r}{\partial\phi^2}$$

$$-\frac{\partial^2\psi_r}{\partial Z^2}-\frac{2}{R}\frac{\partial\psi_z}{\partial Z} \tag{19}$$

$$\nabla^2\psi_\phi=-\frac{\partial^2\psi_\phi}{\partial Z^2}-\frac{\partial^2\psi_\phi}{\partial R^2}-\frac{1}{R^2}\frac{\partial^2\psi_\phi}{\partial\phi^2}$$

$$-\frac{2}{R^2}\frac{\partial\psi_r}{\partial\phi}+\frac{\psi_\phi}{R^2}-\frac{1}{R}\frac{\partial\psi_\phi}{\partial R} \tag{20}$$

$$\nabla^2\psi_z=-\frac{\partial^2\psi_z}{\partial R^2}-\frac{1}{R}\frac{\partial\psi_z}{\partial R}$$

$$-\frac{1}{R^2}\frac{\partial^2\psi_z}{\partial\phi^2}-\frac{\partial^2\psi_z}{\partial Z^2} \tag{21}$$

And the energy equation will be:

$$\left(\frac{1}{R}\frac{\partial\psi_z}{\partial\phi}-\frac{\partial\psi_\phi}{\partial Z}\right)\frac{\partial\theta}{\partial R}+\frac{1}{R}\left(\frac{\partial\psi_r}{\partial Z}-\frac{\partial\psi_z}{\partial R}\right)\frac{\partial\theta}{\partial\phi}$$
$$+\left(\frac{\psi_\phi}{R}+\frac{\partial\psi_\phi}{\partial R}-\frac{1}{R}\frac{\partial\psi_r}{\partial\phi}\right)\frac{\partial\theta}{\partial Z}$$
$$=\frac{l}{r_1}\left[\frac{\partial^2\theta}{\partial R^2}+\frac{1}{R}\frac{\partial\theta}{\partial R}+\frac{1}{R^2}\frac{\partial^2\theta}{\partial\phi^2}+\frac{\partial^2\theta}{\partial Z^2}\right] \quad (22)$$

And the fin equation will be:

$$\frac{\partial\theta}{\partial R}+\frac{\theta}{R}+\frac{1}{R}\frac{\partial\theta}{\partial\phi}+\frac{\partial\theta}{\partial Z}=0 \quad (23)$$

Dimensionless Hydraulic Boundary Conditions

For the vector potential field, the boundary conditions are given as:

$$\frac{1}{R}\frac{\partial}{\partial R}(R\psi_r)=\psi_\phi=\psi_z=0 \qquad at\ R=R_1,1$$

$$\psi_r=\frac{\partial\psi_\phi}{\partial\phi}=\psi_z=0 \qquad at\ \phi=0,\ \pi$$

$$\psi_r=\psi_\phi=\frac{\partial\psi_z}{\partial Z}=0 \qquad at\ Z=0,\ L$$

And for the fin, the boundary conditions are given as:

$$\frac{1}{R}\frac{\partial}{\partial R}(R\psi_r)=\frac{\partial\psi_\phi}{\partial\phi}=\frac{\partial\psi_Z}{\partial Z}=0$$

On the fin faces which were located on the following planes

At R = R_1 *for* $\phi = 0, \pi$ (fin base)

As in **Fig. 3**

At $r = r_1+H_f$ *for* $\phi = 0, \pi$ (fin tip)

At S_1 *and* S_2 *for any r and* ϕ

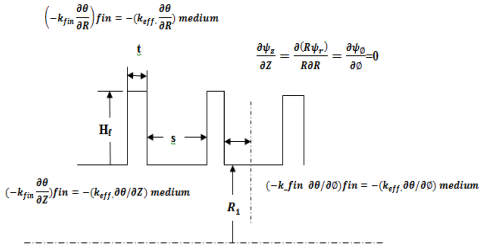

Fig. 3, Fin boundary conditions

Dimensionless Thermal Boundary Conditions

For the temperature field, the dimensionless thermal boundary conditions are:

$$\theta=1 \qquad at\ R=R_1=r_1/r_2$$

$$\theta=0 \qquad at\ R=R_2=1$$

$$\frac{\partial\theta}{\partial\phi}=0 \qquad at\ \phi=0,\ \pi$$

$$\frac{\partial\theta}{\partial Z}=0 \qquad at\ Z=0,\ L$$

$$at\ R=H_1$$

$$-k_{fin}\frac{\partial\theta}{\partial R}\Big|_{fin}=-k_{eff.}\frac{\partial\theta}{\partial R}\Big|_{medium}$$

$at\ S_1$ at any R and ϕ

$at\ S_2$ at any R and ϕ

$$-k_{fin}\frac{\partial\theta}{\partial Z}\Big|_{fin}=-k_{eff.}\frac{\partial\theta}{\partial Z}\Big|_{medium}$$

$at\ \phi = 0,\ \pi$ and any R

$$-k_{fin}\frac{\partial\theta}{\partial\phi}\Big|_{fin}=-k_{eff.}\frac{\partial\theta}{\partial\phi}\Big|_{medium}$$

Where:

$k_{eff.}$ =the effective thermal conductivity of the medium (W/mK).

$$k_{ef}=(1-\varepsilon)\ k_s+\varepsilon\ k_f \quad (24)$$

Computational Technique

Equations (16, 17, 18, 22 and 23) were transformed into the finite difference equations, where the upwind differential method in the left hand side of the energy Eq. (22) and the centered – space differential method for the other terms were used, and solved by using (SOR) method **Wang [5].** A computer program was built using Fortran 90 language to meet the requirements of the problem.

The value of the vector potential ψ will be calculated at each node, in which the value of vector potential is

unknown, the other node will appear in the right hand side of each equation. As an initial value of iteration, zero is chosen for the vector potential field, while a conduction solution is adopted for temperature field. The index (n) was used to represent the nth – approximation of temperature denoted by θ^n and substituted into the approximated equations, which were solved to obtain the nth – approximation of vector potential ψ, then ψ was substituted into Eq. (22) to obtain θ^{n+1}. A similar procedure is repeated until the prescribed convergence criterion given by inequality:

$$Max \left| \frac{\theta^{n+1} - \theta^n}{\theta^n} \right| \leq 10^{-8}$$

was established **Fukuda [1].**

As the steps of iteration increase with Ra^*, a solution obtained for lower Ra^* was used as an initial value of computation for higher Ra^* (double iteration method).

It is clear that as the grid becomes finer, the convergence of the results becomes better. The number of grid points used was 21 grid points in the R – direction, 31 in the ϕ – direction and 301 in the Z – direction which seems reasonable and will be used in the present study. Fig. 4 illustrate the numerical grid in two planes.

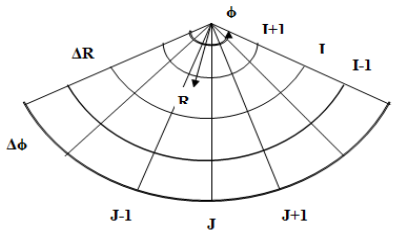

(a) Horizontal (R – ϕ) Plane

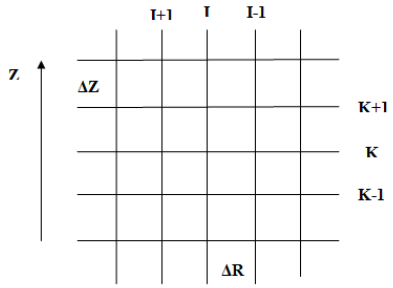

(b) Vertical (R – Z) Plane

Fig. 4, Numerical Grid

Calculation of Local and Average Nusselt Number

Nusselt number is the dimensionless parameter indicative of the rate of energy convection from a surface and can be obtained as follows **Fukuda [1]:**

$$Nu = \frac{q(r_2 - r_1)}{k(T_1 - T_2)} \tag{25}$$

As the local heat flux on the wall is given by:

$$q = -k \frac{\partial T}{\partial r} \tag{26}$$

The local Nusselt number Nu_1 and Nu_2 on the inner and the outer cylinders are written in the form **Fukuda [1]:**

$$Nu_1 = -(1 - R_1) \left(\frac{\partial \theta}{\partial R} \right)_{R=R_1} \tag{27}$$

$$Nu_2 = -(1 - R_1) \left(\frac{\partial \theta}{\partial R} \right)_{R=1_1} \tag{28}$$

The average Nusselt number Nu_{in} and Nu_{out} on the inner and the outer cylinders are defined as:

$$Nu_{in} = -(1 - R_1) \frac{1}{\pi L} \int_0^L \int_0^\pi \left(\frac{\partial \theta}{\partial R} \right)_{R=R} d\phi \, dZ \tag{29}$$

$$Nu_{out} = -(1 - R_1) \frac{1}{\pi L} \int_0^L \int_0^\pi \left(\frac{\partial \theta}{\partial R} \right)_{R=1} d\phi \, dZ \tag{30}$$

Results and Discussion

Figs. 5 to 8 show the variation of the average Nusselt number on the hot cylinder with Ra^* for different radius ratios, without and with fins respectively. These figures show that for any radius ratio, the average *Nu* is generally constant for low values of Ra^* then as Ra^* reached nearly 100, *Nu* increased with increasing Ra^*. These values increased as *Rr* decreased due to the enlarge of the distance between the two cylinders. For low values of Ra^*, the maximum values of *Nu* was for maximum *Rr* until Ra^* reached nearly 100, then the situation would inverse and the maximum values of *Nu* would be for minimum *Rr* which improved that for low values of Ra^* the heat transferred by conduction and as Ra^* increased the convection heat transfer and that would be the dominant. These figures show as Ra^* exceeds 100, as H_f increases *Nu* decreases and decreasing the pitch (by increasing fin numbers) causes *Nu* to decrease.

Fig. 9 illustrates that the values of the average Nusselt number was low for high radius ratio; then they increased with high intensity as radius ratio decreased. When the annulus gap decreased, the resistance to the circulation motion of the convection cells increased and this lead to slower replacement of the hot air adjacent to the inner surface by the cold air adjacent to the outer surface and these resulted in an increase in the average temperature of the annulus inner surface and consequently in a decrease in the rate of heat transfer. It is clear that the curves of the different radius ratios converge to each others as Ra^* decreases; this means that the effect of radius ratio on the rate of heat transfer decreases with decreasing Ra^*. This can be attributed to that as Ra^* decreases the heat convection becomes insignificant, or in other words, heat conduction becomes the dominant heat transfer in the fluid layer.

Convective heat transfer rate is controlled by three parameters (h, A and ΔT), according to

$$Q = h_i \; A_{in}(T_1 - T_2) = h_o \; A_{out}(T_1 - T_2)$$

For the same modified Rayleigh number (i.e. ΔT is constant), dQ/Q=(dA/A)+(dh/h). If the increase in the surface area is more than the decrease in the heat transfer coefficient (average *Nu*), the total heat transfer rate will increase, or if the decrease in the heat transfer coefficient is more than the increase in the surface area, the total heat transfer rate will decrease **Harith [7].**

Fig. 10 indicates that there is a reduction in the average Nusselt number with increasing H_f from 3mm to 11mm. For the same value of Ra^*, reduction in the average Nusselt number may be ranged between (18% to 38 %).

Figs. 11 to 13 indicate that there is a reduction in the average Nusselt number with increasing the number of fins from n=12(pitch=19.2mm) to n=23(pitch=8.4 mm) and then to n=45(pitch=3mm) with the increasing of inclination angle, radius ratio and fin length.

The distribution of the local Nusselt number are shown in **Fig. 14.**The peak of the local Nu on the outer cylinder wall generally appeared at a position of Z=L (at the top) and ϕ with some deviation from π. while for the inner cylinder the peak appeared at a position of Z=0 (bottom of the cylinder).

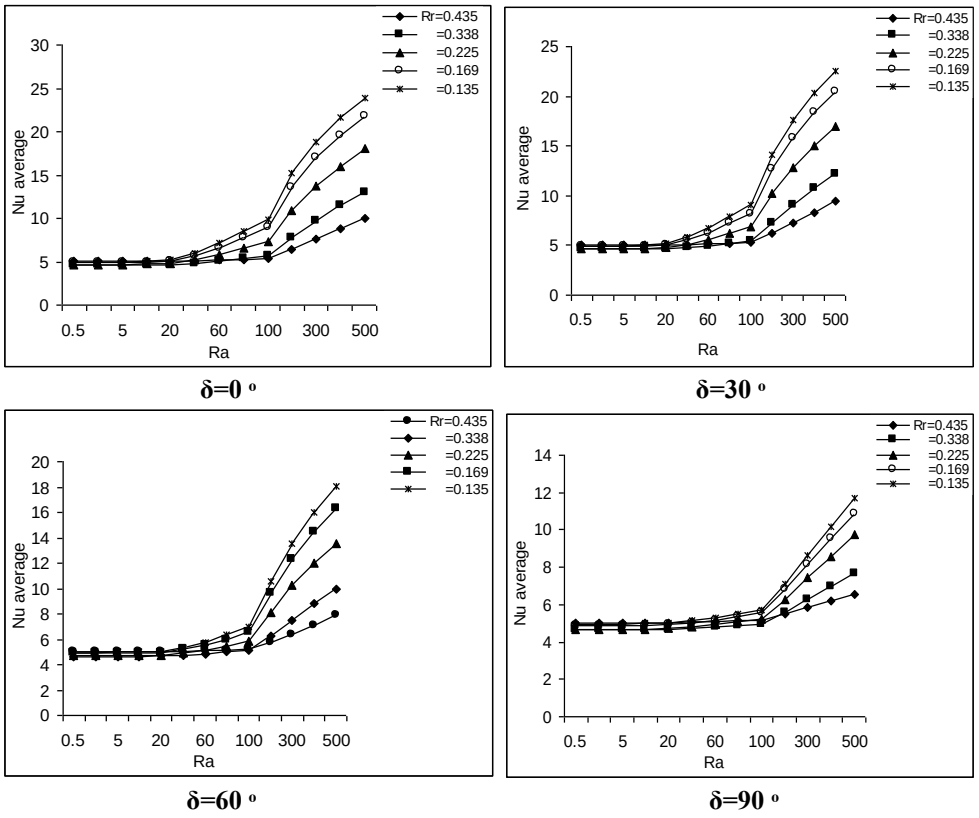

Fig. 5, Variation of average Nusselt number with Ra^* on the hot cylinder for n=0 and for different values of Rr and δ

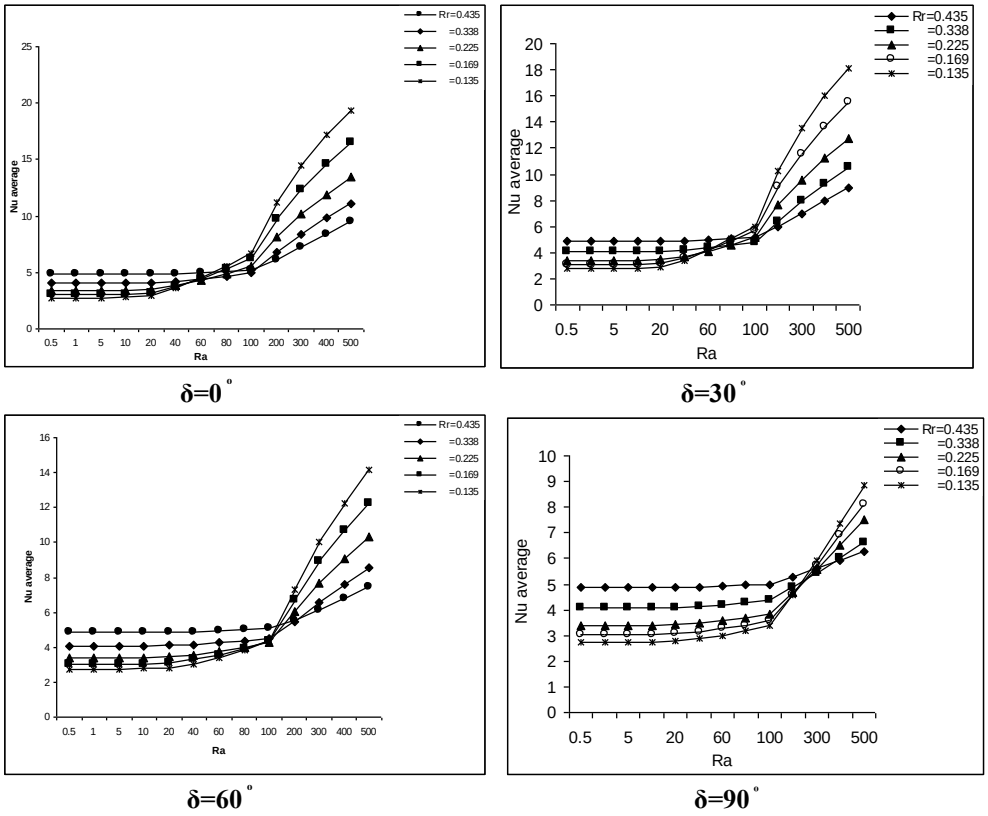

Fig. 6, Variation of average Nusselt number with Ra^* on the hot cylinder for n=12, H_f=3mm and for different Rr, δ

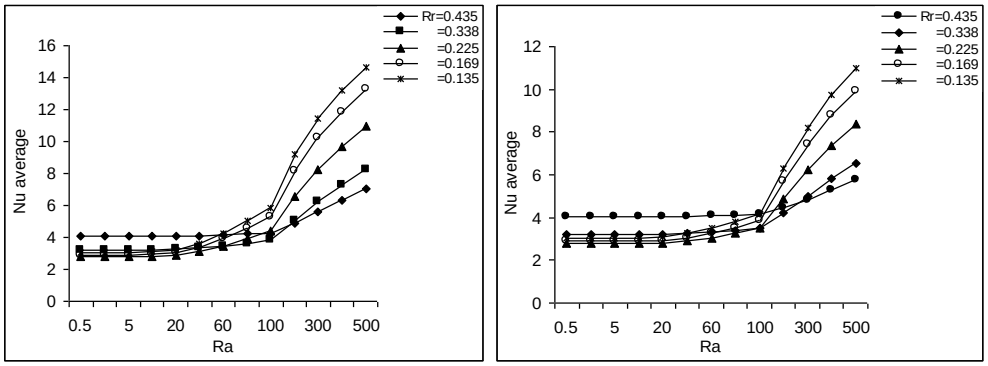

H_f=7mm, δ=0° **H_f=7mm, δ=60°**

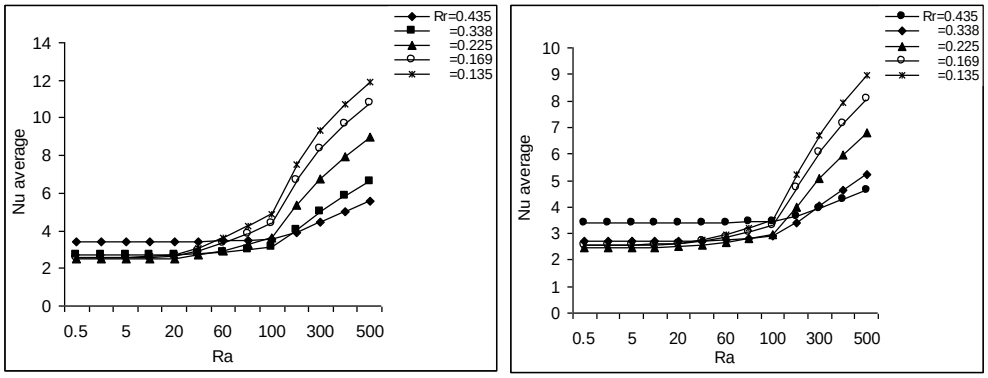

H_f=11mm, δ=0° **H_f=11mm, δ=60°**

Fig. 7, Variation of average Nusselt number with Ra^* on the hot cylinder for n=12and for different Rr and δ

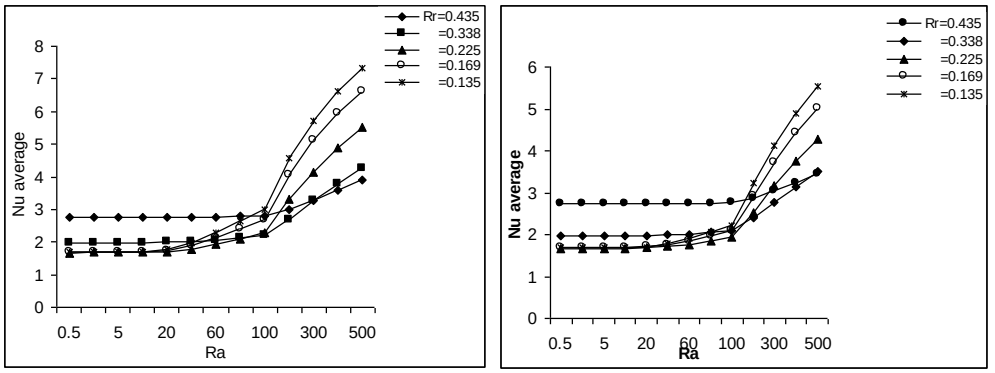

n=23, δ=0° **n=23, δ=60°**

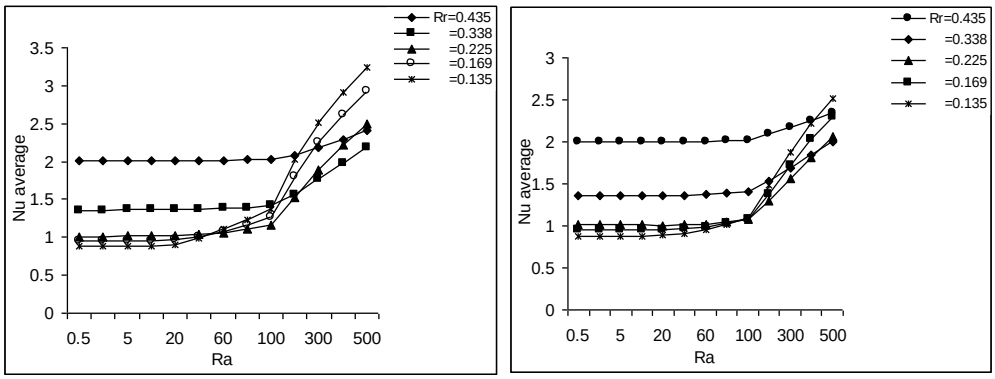

n=45, δ=0° **n=45, δ=60°**

Fig. 8, Variation of average Nusselt number with Ra^* on the hot cylinder for H_f=11mm and for different Rr

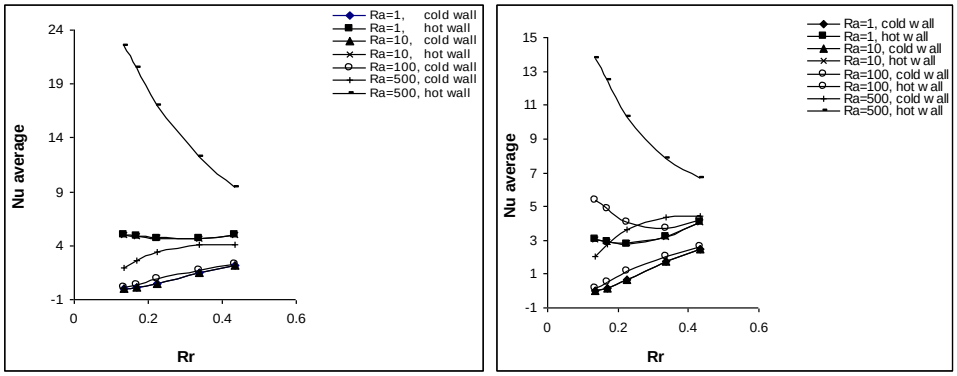

n=12

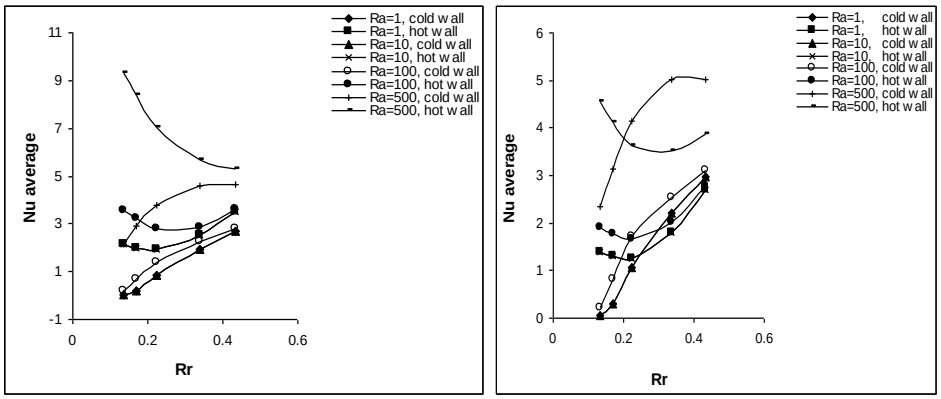

n=23 **n=45**

Fig. 9, Variation of average Nusselt number with Rr for H_f=7mm δ =30° and for different Ra^*

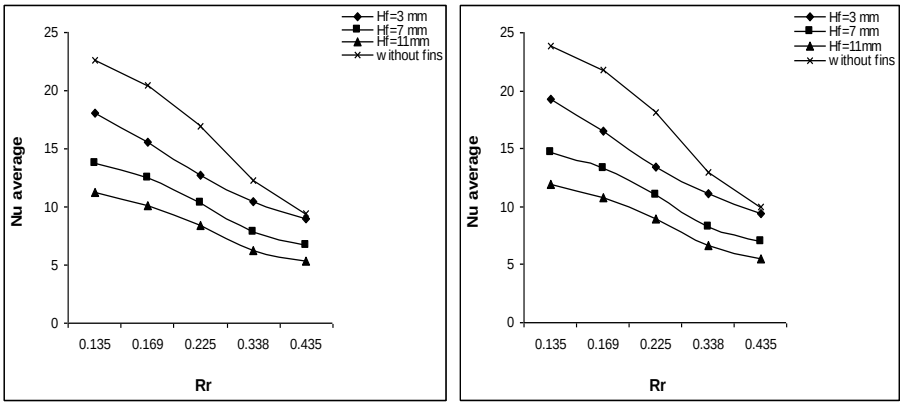

δ=0° **δ=30°**

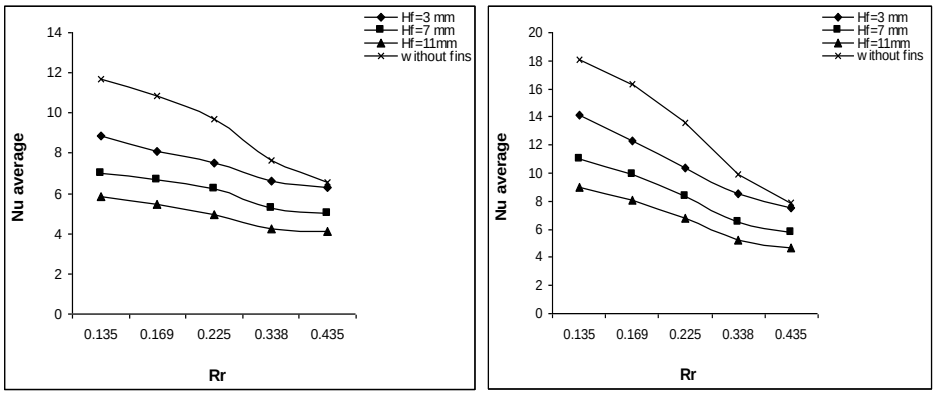

δ=60° **δ=90°**

Fig. 10, Variation of average Nusselt number with Rr for Ra^*=500, n=12 and for different H_f and δ

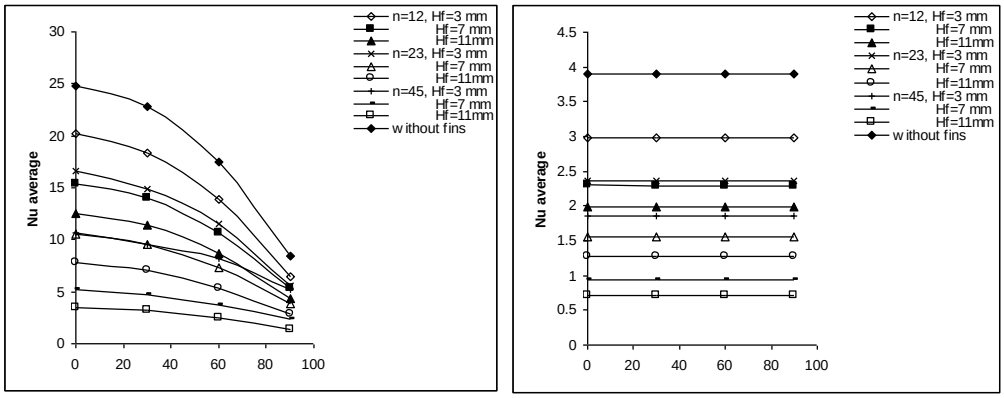

Ra^*=500 **Ra^*=1**

Fig. 11, Variation of average Nusselt number with δ for Rr=0.435 and for different n and H_f

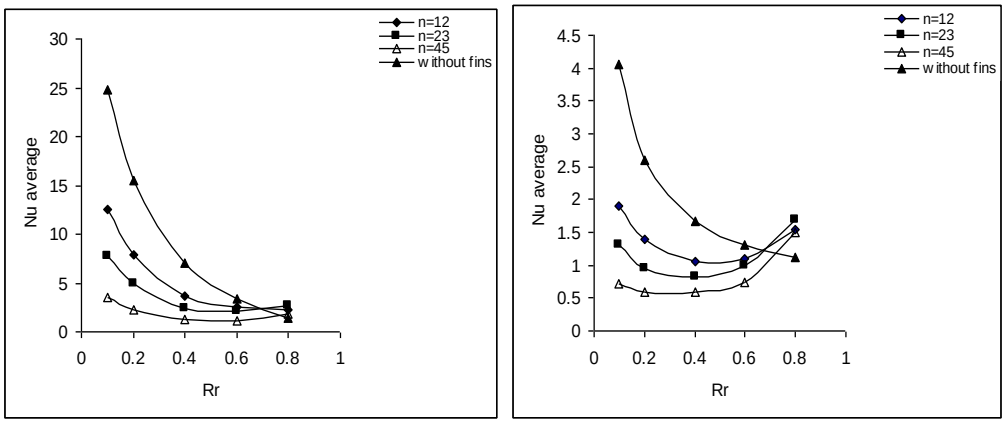

Ra^*=500 **Ra^*=10**

Fig. 12, Variation of average Nusselt number with Rr for δ =0, H_f=11mm and for different n and Ra

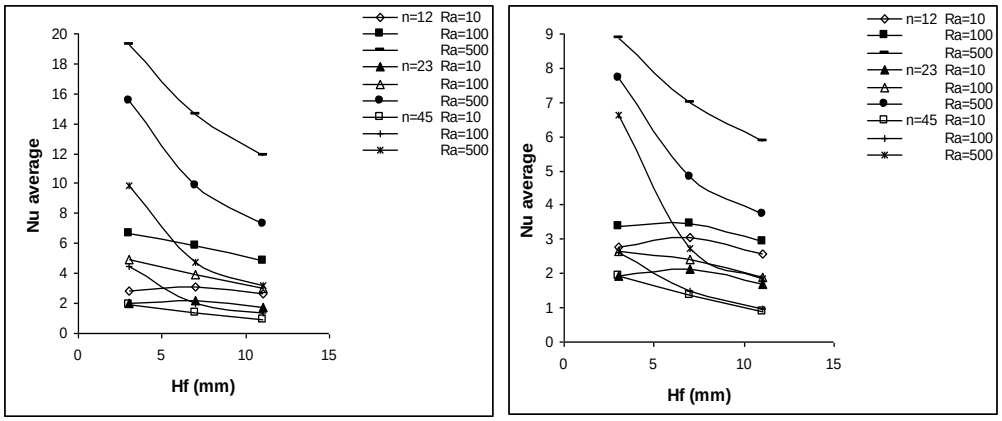

δ=0° **δ=90°**

Fig. 13, Variation of average Nusselt number with H_f and for Rr=0.135 and different n and Ra^*

Fig. 15 illustrate the relation between the average Nusselt number and modified Rayleigh number for different Rr and δ for n=12 and H_f=3mm. The average Nusselt number was nearly constant because of the predominance of conduction mode on heat transfer process. For Ra^*>100 (in the numerical part) convection became predominant mechanism and the average Nusselt number began to clearly increase.

Most of the experimental values were lower than that of the numerical; one

of the reasons may be the conduction losses through the sides and hence the absence of perfectly insulated ends boundaries and may be because of the assumptions which had been taken and this is true even for this research or for [**Prasad and Kulacki 1985] and [Havstad and Burns 1982]** .

A comparison for the variation of the average Nusselt number on the inner and outer cylinders with Ra^* was made with that of **Fukuda[1]** in **Fig. 16** and its clear that Nu is constant for low values of Ra^*, until Ra^* equal nearly 100, then Nu will increase with the increasing of Ra^* as presented in this work.

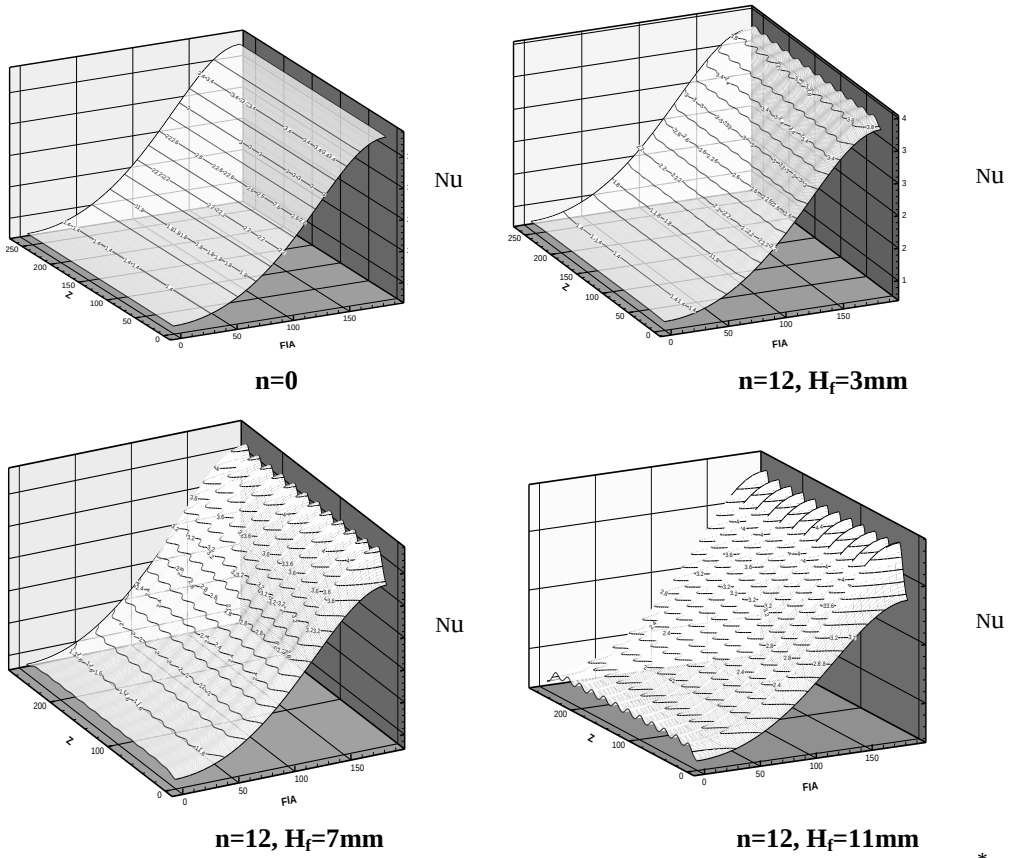

Fig. 14, The distribution of local Nusselt number in ϕ and Z – direction for $Ra^*=100$ and $\delta=0^o$

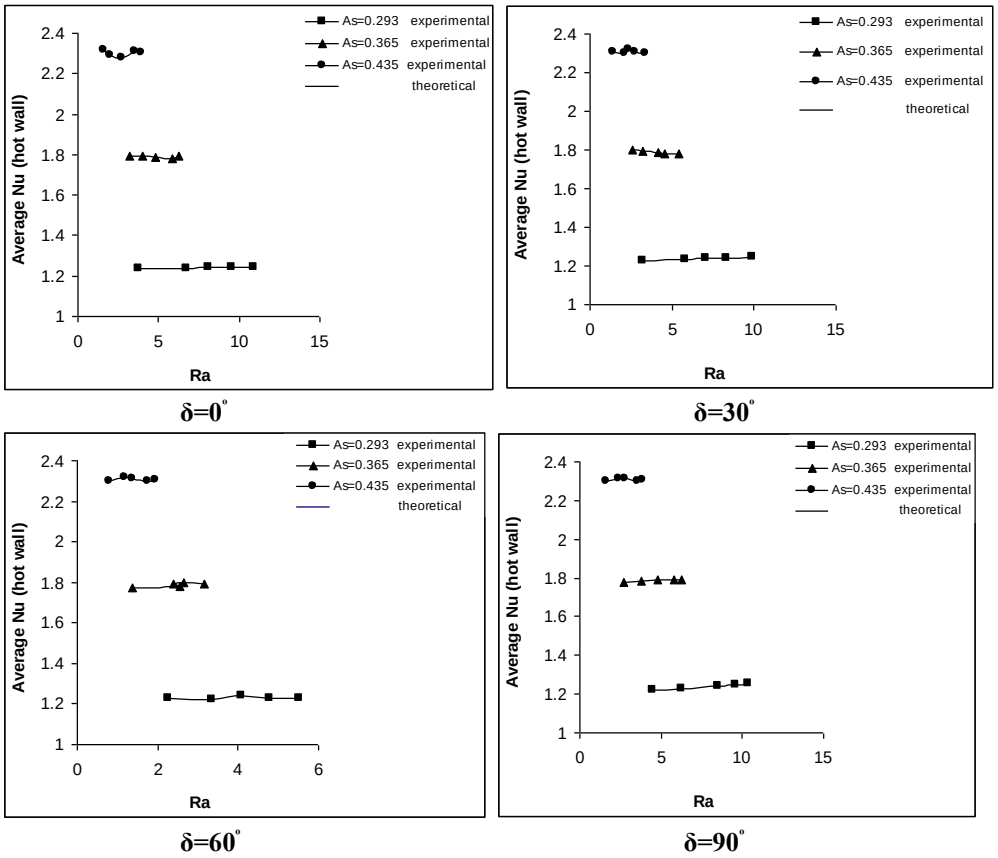

Fig. 15, Variation of average Nusselt number with modified Ra for different Rr and δ for n=12, H_f =3mm

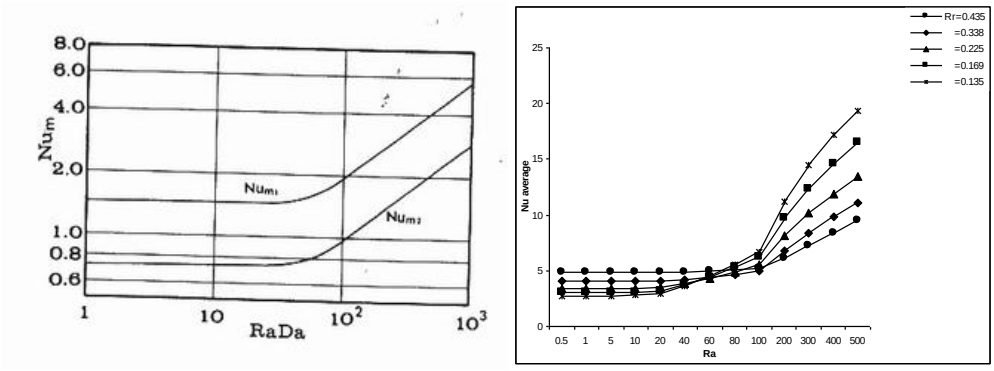

Fukuda[1] **Present Work**

Fig. 16, A comparison for the variation of the average Nusselt with Ra^* for Fukuda[1] with that of the present work respectively

Conclusions

The following major conclusions can be drawn from the experimental and numerical study:

1- Average Nu number increases with increasing fin length at the same Ra^* and fin number unless the surface area of the inner cylinder exceeds that of the outer cylinder, then the heat will be stored in the porous media.

2- There is a reduction in the average Nusselt number with increasing the number of fins and with the increasing of inclination angle, radius ratio and fin length.

3- For all parameters, results showed that the average Nu number increases with an increase in modified Rayleigh number and

hardly affected by δ for low values of Ra^*.

4- Increasing Rr cause a clearly increase in average Nusselt number for $Ra^* > 100$.
5- The peak of the local Nu on the outer cylinder wall generally appeared at a position of Z=L (at the top) and ϕ with some deviation from π. while for the inner cylinder the peak appeared at a position of Z=0 (bottom of the cylinder).

References

1- Fukuda K., Takata Y., Hasegawa S., Shimomura H. and Sanokawa K., "Three – Dimensional Natural Convection in a Porous Medium Between Concentric Inclined Cylinders", Proc. 19th Natl Heat Transfer Conf., Vol. HTD – 8, pp. 97 – 103, 1980.
2- Bogdan I. Pavel and Abdulmajeed A. Mohamad, 2004 "An Experimental and Numerical Study on Heat Transfer Enhancement for Gas Heat Exchangers Fitted with Porous Media", Int. J. of Heat and Mass Transfer Vol. 47, pp. 4939–4952. www.elsevier.com.
3- Ramón L. F. and Sergio G. M., 2007 "Three Dimensional Natural Convection in Finned Cubical Enclosure", Int. J. of Heat and Fluid Flow. Vol. 28, pp. 289-298.
4- Nield D. A. and Bejan A., 1999 "Convection in Porous Media", Springer-Verlag, New York.
5- Wang Bu – Xuan and Zhang Xing, 1990 "Natural Convection in Liquid Saturated Porous Media Between Concentric Inclined Cylinders" Int. J. Heat and Mass Transfer Vol. 33. No 5, pp. 827-833.
6- Aziz K. and Hellums J. D., 1967 "Numerical Solution of the Three Dimensional Equations of Motion for Laminar Natural Convection", The Physics of Fluids, V0l. 10, No. 2, pp. 314 – 324.
7- Harith H. H., 2009 "An Investigation of Fins Geometry Effects for Laminar Free Convection in Horizontal Annulus with Finned Inner Cylinder", Msc Thesis, University of Baghdad.
8- Prasad, V. and Kulacki, F. A., "Natural Convection in Porous Media Bounded by Short Concentric Vertical Cylinders", Transaction of ASME, J. of Heat Transfer , Vol. 107, pp. 147-154, February, 1985.
9- Havstad M.A., Burns P.J.," Convective Heat Transfer in Vertical Cylindrical Annuli Filled with a Porous Medium", Int. J. Heat and Mass Transfer, Vol. 25, No.11, pp. 1755-1766, 1982

Nomenclature

Greek Symbols

Symbol	Description	Unit
α	Thermal diffusivity	m^2/s
β	Volumetric thermal expansion coefficient	1/K
δ	Angle of inclination	degree
θ	Dimensionless temperature	-
υ	Kinematic viscosity of fluid	m^2/s
μ_f	Dynamic viscosity of fluid	$N.s/m^2$

Latin Symbols

Symbol	Description	Unit
C_p	Specific heat at constant pressure	kJ/kg°C
FIA	Φ in Fig. 13	-
g	Acceleration due to gravity	m/s^2
H_f	Fin length	m
k_f	Thermal conductivity of the fluid	W/m K
k_s	Thermal conductivity of the solid	W/m K
$K_{eff.}$	Effective thermal conductivity of the porous media	W/m K
K	Permeability	m^2
l	Cylinder length	m
L	Dimensionless cylinder length	-
Nu_1	Local Nusselt number on the inner cylinder	-
Nu_2	Local Nusselt number on the outer cylinder	-
p	Pressure	N/m^2
q	Local heat flux	W
r	Radial coordinate	m
R	Dimensionless radial coordinate	m
Symbol	**Description**	**Unit**
Ra^*	Modified Rayleigh number	-
Rr	Radius ratio	-
S	Fin pitch	m
T	Temperature	K
t	Fin thickness	m
u_r, u_ϕ, u_z	velocity component in r,ϕ and z - direction	m/s
U_r, U_ϕ, U_z	Dimensionless velocity component in R, ϕ and Z direction	-
x, y, z	Cartesian coordinate system	m
Z	Dimensionless axial coordinate	-